ACCSCIENCE PUBLISHING

An International Journal of Optimization and Control: Theories & Applications
ISSN: 2146-0957 eISSN: 2146-5703
Vol.X, No.X, pp.X-X (2026)
https://doi.org/10.36922/IJOCTA026340217

IJOCTA

RESEARCH ARTICLE

An analytical-computational method for parameter optimization of hyperbolic electrostatic energy analyzers

Arman Saulebekov[1], Zhanar Kambarova[2]*, Meiramkul Tungushbekova[2], and Tilektes Shugayeva[3]

[1]Department of Mathematical Modeling, Kazakhstan Branch of Lomonosov Moscow State University, Astana, Kazakhstan

[2]Department of Physics and Nanotechnology, Faculty of Physics and Technology, Buketov Karaganda National Research University, Karaganda, Karaganda Region, Kazakhstan

[3]Global College, Heriot-Watt University Aktobe Campus, K. Zhubanov Aktobe Regional University, Aktobe, Aktobe Region, Kazakhstan

saulebekovarman@gmail.com, kambarova_zhanar@buketov.edu.kz, tungushbekova_meiramkul@buketov.edu.kz, tshugayeva@zhubanov.edu.kz

ARTICLE INFO

Article history:
Received: August 17, 2026
Revised: October 24, 2026
Accepted: October 26, 2026
Published Online: November 18, 2026

Keywords:
Hyperbolic electrostatic field
Charged-particle energy analyzer
Analytical modeling
Parameter optimization
Successive approximation

AMS Classification 2010:
49M30, 78A15, 34A45

ABSTRACT

Hyperbolic electrostatic mirrors are promising elements of compact high-luminosity charged-particle energy analyzers, but their operating parameters are usually determined through extensive numerical trajectory calculations. For a hyperbolic mirror placed between two cylindrical mirror stages, with the beam entering and exiting through the hyperbolic electrode, analytical first-order focusing and collimation conditions have not been reported. This paper presents an analytical-computational method for determining the parameters of such a mirror. Closed-form solutions of the equations of motion are obtained for the axially symmetric hyperbolic field, and their differentiation with respect to the entrance angle yields explicit first-order sensitivity relations for the exit coordinate and exit angle, from which the focusing and collimation conditions are formulated. A geometric pre-screening of the straight-line trajectory segments in the field-free region excludes parameter combinations for which the beam cannot enter the field or leave it symmetrically; for the electrode parameter $\mu = 0.8$, admissible entrance conditions exist only for normalized beam offsets $b < \mu$. The remaining transcendental equations are solved using successive approximations within this reduced domain. For a fixed entrance point, the exit coordinate decreases with increasing entrance angle and electrode parameter. The method replaces broad numerical scanning with analytical screening followed by low-dimensional iteration and provides initial approximations for designing cylindrical–hyperbolic–cylindrical analyzers for space and plasma diagnostics.

CC BY

1. Introduction

Electrostatic mirrors are widely used in charged-particle energy analyzers because their field geometry can provide strong energy dispersion and angular focusing while maintaining high particle-beam transmission. Among them, the hyperbolic electrostatic mirror (HM) is of particular interest owing to the strongly non-uniform structure of its electrostatic field and its pronounced dispersive properties, making it a promising element for compact, high-luminosity charged-particle energy analyzers. In the configuration considered in this study, the HM operates as an intermediate element between two cylindrical mirror stages, forming a cylindrical–

*Corresponding Author

hyperbolic–cylindrical mirror system in which the beam enters and exits the field through the hyperbolically shaped electrode itself.

However, the practical use of HM in this configuration is hindered by the difficulty of determining its operating parameters. The electrode curvature, beam entrance angle, and beam position must be chosen so the beam can enter and leave the field through the hyperbolic electrode and, at the same time, satisfy the first-order focusing or collimation conditions. In the absence of explicit relations between these parameters, they have to be identified through extensive numerical trajectory calculations over a multidimensional parameter space.

A combined electrostatic energy analyzer composed of successively arranged hyperbolic and cylindrical mirrors was proposed and theoretically substantiated by Ashimbaeva *et al.*,[1] where schemes providing angular second-order focusing, high luminosity, and an exit angle of 90° were obtained, with a relative energy resolution ($\Delta E/E$) of 0.28%. In that work, the beam entered and exited through the conical electrode, whereas in the present case it does so through the hyperbolic electrode. Building on this line of analytical treatment of combined mirror systems, Kambarova *et al.*[2] proposed an electron-optical scheme of a mirror energy analyzer based on an axially symmetric octupole-cylindrical field and derived an integro-differential equation of charged-particle motion, solved via a fractional-power series expansion. Together, these works[1,2] demonstrate the continued relevance of approximate analytical methods for the design of high-luminosity charged-particle energy analyzers. A related design based on the superposition of a cylindrical field and a second-type axial dodecapole was subsequently proposed by Kambarova *et al.*,[3] who developed the electron-optical scheme through numerical modeling and showed that the resulting analyzer combines high energy resolution with effective luminosity, making it suitable for charged-particle beam diagnostics in space applications. This body of work confirms that combining simple axially symmetric field components—whether analytically or numerically—remains an effective strategy for achieving high-luminosity, high-resolution energy analyzers.

Beyond mirror-type energy analyzers, analytical descriptions of electrostatic fields remain an active area of research for a broader class of instruments. Spivak-Lavrov *et al.* recently derived explicit analytical expressions for the potentials and field derivatives of quadrupole, sextupole, and octupole systems based on a conducting circular cylinder, confirming that closed-form analytical solutions, where obtainable, continue to offer advantages over purely numerical approaches to electrostatic field synthesis, such as the finite-element method (FEM), finite-difference method (FDM), and boundary element method (BEM), which are widely used for field calculation and charged-particle-optical simulation.[5,6] A similar advantage of closed-form solutions was demonstrated by Vallette and Indelicato,[7] who derived an analytical expression for the on-axis potential of an electrostatic ion beam trap using conformal mapping, noting that finite-element calculations were impractically slow for exploring the large parameter space required to tune such traps.

Closely related to the present work, Gonzalez-Lizardo *et al.*[8] simulated a hyperbolic field energy analyzer, in which the hyperbolic potential is formed near a diaphragm between conical electrodes, using a fully numerical approach: the electric field was computed on a three-dimensional grid and particle trajectories were obtained by direct kinematic integration. While this confirms the practical relevance of hyperbolic-field analyzers for plasma and energy diagnostics, it also highlights the absence of an analytical treatment of the focusing conditions in this closely related configuration. The same is true of the earliest hyperbolic-lens studies, where hyperbolic equipotential surfaces were shown to provide simultaneous spatial focusing and retarding potential selection for high-density plasma diagnostics and particle beam focusing,[9] but again without an analytical focusing framework.

The demand for fast field-calculation methods is also evident in electrostatic lens optimization, where thousands of field evaluations are needed in genetic-algorithm-based design loops. Hesam Mahmoudi Nezhad *et al.*[10] proposed a fourth-order electrode method achieving FEM-like accuracy at a fraction of the cost, while Yao *et al.*[11] combined the BEM with adaptive trajectory integration, achieving a 10–100-fold speed-up that was validated experimentally. Optimization of the geometrical parameters of conventional cylindrical mirror analyzers has likewise been shown to provide substantial improvements in energy resolution.[12] More generally, successive-approximation techniques have a well-established basis in charged-particle optics, where nonlinear contributions to particle motion can be evaluated

iteratively,[13] and recent studies have integrated trajectory calculations with global optimization techniques such as genetic algorithms and particle swarm optimization to determine electrostatic-lens geometries with improved optical characteristics.[14] Together, these developments confirm that the trade-off between speed and accuracy remains central to electron-optical design, further motivating the use of analytical solutions, such as the one presented here, wherever attainable.

This same trade-off is visible across other classes of charged-particle instruments, where numerical optimization and trajectory search have largely replaced closed-form analysis. In hemispherical deflector analyzers, BEM- and FDM-based calculations have been used to optimize fringing-field conditions and achieve first-order focusing,[15] and a genetic-algorithm approach was applied by Isik and Ince[16] to optimize electron-trajectory focusing, showing faster convergence than conventional field calculations. Numerical search procedures have also been developed for determining focusing conditions in charged-particle optical systems directly from trajectory-analysis data, allowing the central trajectory parameter and focal position to be identified without a closed-form solution of the complete system;[17] the present study instead exploits an analytical trajectory description to derive first-order sensitivity relations explicitly and restrict the iterative search to a geometrically admissible domain. In mass spectrometry, similar numerical and semi-analytical strategies have been used to predict transmission efficiency and mass bias in time-of-flight instruments,[18] to optimize collimating systems against axial aberration,[19] to validate aberration theory against simulations performed with the SIMION ion-optics software for sector-field analyzers,[20] to conduct multi-criteria random-search optimization of magnetic mass-analyzer schemes,[21] to construct Mathieu stability plots for toroidal ion traps from computed multipole coefficients,[22] and to replace hyperbolic electrodes with manufacturable ladder-shaped structures optimized by numerical field simulation.[23] In contrast to these approaches, which rely on repeated numerical field or trajectory evaluations (FEM, FDM, BEM, SIMION) or on stochastic global search (genetic algorithms, particle swarm optimization, random search), the present method uses closed-form trajectory solutions, analytically derived first-order sensitivities, and a deterministic successive-approximation procedure applied within a geometrically pre-screened domain. Once the admissible configurations are identified, their final selection becomes a multi-criteria problem, since energy resolution, luminosity, and instrument size must be balanced. For such problems, recent optimization studies have proposed general decision-making tools, including Archimedean t-norm-based q-rung orthopair fuzzy Hamy mean operators with ordinal priority weights[24] and large language model-assisted Z-number multi-agent frameworks for expert weight elicitation,[25] which could be used to rank the admissible analyzer configurations obtained with the present method.

Thus, although a wide range of numerical tools is available in charged-particle optics, a gap remains for the HM considered here: to the best of our knowledge, the first-order focusing and collimation conditions for a hyperbolic mirror in which the beam enters and exits through the hyperbolically shaped electrode have not been formulated analytically. This gap has three main causes. First, the analytical treatment of the combined mirror system[1] assumed that the beam crosses the conical electrode, which is a straight line in the meridional plane. When the beam crosses the hyperbolic electrode instead, the entrance and exit points lie on a curved surface, the boundary conditions change, and the focusing conditions obtained in that work cannot be applied. Second, the existing studies of hyperbolic-field analyzers[8,9] have relied on numerical field computation and direct trajectory integration; they confirm the practical relevance of such analyzers but do not provide explicit relations between the electrode geometry, the entrance conditions, and the trajectory coordinates. Third, the fast numerical and optimization methods reviewed above[10-17] reduce the cost of individual field or trajectory evaluations but do not reduce the search domain itself, so geometrically inadmissible configurations, in which the beam cannot enter or leave the field through the hyperbolic electrode, are still evaluated alongside feasible ones. As a consequence, determining the operating regimes of such an HM remains a broad parameter-search problem.

This leads to the following research question: can the first-order focusing and collimation conditions of an HM with the beam passing through the hyperbolic electrode be expressed in explicit analytical form and used to determine its operating parameters within a geometrically admissible domain, without broad numerical scanning? To address this question, the present study develops an analytical-computational

framework that combines an exact description of the field and particle trajectories with geometric reduction of the parameter space and a successive-approximation procedure. The main contributions of this work are: (i) analytical relations describing charged-particle trajectories in the hyperbolic electrostatic field; (ii) first-order differential relations required for angular focusing and beam-collimation analysis; (iii) identification of a reduced admissible parameter domain through preliminary geometrical trajectory analysis; and (iv) low-dimensional iterative parameter-search algorithms for determining operating points satisfying the prescribed first-order angular-focusing and collimation conditions.

2. Mathematical model

Figure 1 shows the HM considered in this study. The axially symmetric field of the HM is formed by rotation, about the z-axis, of two conical electrodes 1 and 2 held at a potential of the same sign as the charge of the analyzed particles, and a hyperbolically shaped electrode 3 that is grounded.

The asymptotes of the hyperbolic electrode are inclined at an angle $\beta = \arctan\sqrt{2} = 54.74°$ with respect to the z-axis.

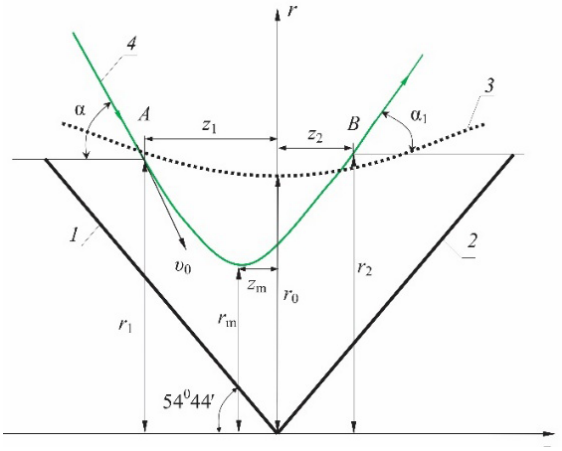


Figure 1. Geometry and charged-particle trajectories in the hyperbolic electrostatic mirror: 1, 2 are the conical electrodes; 3 is the hyperbolic electrode in the rz plane; 4 is the charged-particle trajectories; A, B are the entrance and exit points, respectively; α, α_1 are the entrance and exit angles, respectively; r_m, z_m are the coordinates of the turning point; and r, z are the cylindrical coordinates.

2.1. Hyperbolic electrostatic field

Consider the following form of the electrostatic potential:

$$U = -a\left(\frac{r^2}{2} - z^2\right) + C \tag{1}$$

Assuming that $U = 0$ at $r = r_0$ and $z = 0$, the integration constant is $C = \frac{ar_0^2}{2}$, and the potential distribution takes the following form:

$$U = -a\frac{r^2 - r_0^2}{2} + az^2 \tag{2}$$

For $U = 0$, the corresponding equipotential surface is described by

$$r^2 = 2z^2 + r_0^2 \tag{3}$$

2.2. Charged-particle equations of motion

The equations of motion of a charged particle in the considered electrostatic field can then be written as:

$$\left.\begin{aligned} E_r &= -\frac{\partial U}{\partial r} = ar, m\ddot{r} = aer \\ E_z &= -\frac{\partial U}{\partial z} = -2az, m\ddot{z} = -2aez \end{aligned}\right\} \tag{4}$$

Multiplying the last two terms in **Equation 4** by $\dot{r}$ and $\dot{z}$, respectively, and integrating each equation once yields:

$$\left.\begin{aligned} \dot{r}^2 &= \frac{ea}{m}r^2 + C_1 \\ \dot{z}^2 &= -\frac{2ea}{m}z^2 + C_2 \end{aligned}\right\} \tag{5}$$

At point A, where the charged-particle beam enters the electrostatic field (**Figure 1**), the radial velocity component $\dot{r}_A$ is $-\upsilon_0 \sin\alpha$ and the axial velocity component $\dot{z}_A$ is $\upsilon_0 \cos\alpha$. Substitution of these initial conditions into **Equation 5** yields:

$$\left.\begin{aligned} \dot{r}^2 &= \frac{ea}{m}\left(r^2 - r_1^2\right) + \upsilon_0^2 \sin^2\alpha \\ \dot{z}^2 &= -\frac{2ea}{m}\left(z_1^2 - z^2\right) + \upsilon_0^2 \cos^2\alpha \end{aligned}\right\} \tag{6}$$

From **Equation 6**, we obtain the derivative $\frac{dr}{dz}$ required for the subsequent analysis:

$$\frac{dr}{dz} = \pm\frac{\sqrt{\frac{m\upsilon_0^2}{2ea}\sin^2\alpha + \frac{r^2}{2} - \frac{r_1^2}{2}}}{\sqrt{\frac{m\upsilon_0^2}{2ea}\cos^2\alpha + z_1^2 - z^2}} \tag{7}$$

where the minus sign corresponds to the

descending branch of the trajectory and the plus sign corresponds to its ascending branch.

For convenience, the following normalized parameters are introduced:

$$S=\sqrt{\frac{W}{ea}}\sin\alpha, q=\sqrt{\frac{W}{ea}}\cos\alpha \tag{8}$$

where $W=\frac{mv_0^2}{2}$. Using the introduced parameters, **Equation 7** can be rewritten in the simplified form:

$$\pm\sqrt{2}\frac{dr}{\sqrt{2S^2-r_1^2+r^2}}=\frac{dz}{\sqrt{q^2+z_1^2-z^2}} \tag{9}$$

At the turning point of the trajectory, $\frac{dr}{dz}=0$. Therefore:

$$\begin{aligned}&2S^2-r_1^2+r_m^2=0 r_m^2=r_1^2-2S^2\\&=2z_1^2+r_0^2-2S^2\end{aligned} \tag{10}$$

Equation 9 is then integrated separately over the descending and ascending branches of the trajectory. For the descending branch, the integration limits extend from r_1 to r_m, whereas for the ascending branch they extend from r_m to r_1:

$$\begin{aligned}&-\sqrt{2}\int_{r_1}^{r_m}\frac{dr}{\sqrt{2S^2-r_1^2+r^2}}+\sqrt{2}\int_{r_m}^{r_2}\frac{dr}{\sqrt{2S^2-r_1^2+r^2}}\\&=\int_{z_1}^{z_2}\frac{dz}{\sqrt{q^2+z_1^2-z^2}}\end{aligned} \tag{11}$$

Using standard integrals, the first integral can be evaluated as:

$$\int\frac{dr}{\sqrt{r^2-\left(r_1^2-2S^2\right)}}=\ln\left|r+\sqrt{r^2-r_m^2}\right| \tag{12}$$

where $r_1^2-2S^2=r_m^2>0$. Similarly, the second integral is obtained as:

$$\int\frac{dz}{\sqrt{q^2+z_1^2-z^2}}=\arcsin\frac{z}{\sqrt{q^2+z_1^2}} \tag{13}$$

where $z^2<q^2+z_1^2$. Thus, it follows from **Equation 11** that:

$$\begin{aligned}&\sqrt{2}\left\{\int_{r_m}^{r_1}\frac{dr}{\sqrt{2S^2-r_1^2+r^2}}+\int_{r_m}^{r_2}\frac{dr}{\sqrt{2S^2-r_1^2+r^2}}\right\}\\&=\int_{z_1}^{z_2}\frac{dz}{\sqrt{q^2+z_1^2-z^2}}\end{aligned} \tag{14}$$

$$\begin{aligned}&\sqrt{2}\left\{\ln(r+\sqrt{r^2-r_m^2})\Big|_{r_m}^{r_1}+\ln(r+\sqrt{r^2-r_m^2})\Big|_{r_m}^{r_2}\right\}\\&=\arcsin\frac{z}{\sqrt{q^2+z_1^2}}\Bigg|_{z_1}^{z_2}\end{aligned} \tag{15}$$

$$\begin{aligned}&\sqrt{2}\left\{\ln\frac{r_1+\sqrt{r_1^2-r_m^2}}{r_m}+\ln\frac{r_2+\sqrt{r_2^2-r_m^2}}{r_m}\right\}\\&=\arcsin\frac{z_2}{\sqrt{q^2+z_1^2}}-\arcsin\frac{z_1}{\sqrt{q^2+z_1^2}}\end{aligned} \tag{16}$$

According to the equation of the equipotential surface, **Equation 3**, and **Equation 10**, the following expressions are obtained:

$$\begin{aligned}&r_1^2=2z_1^2+r_0^2,\ r_2^2=2z_2^2+r_0^2,\ r_1^2-r_m^2=2S^2,\\&r_1+\sqrt{r_1^2-r_m^2}=\sqrt{2z_1^2+r_0^2}+\sqrt{2}S\end{aligned} \tag{17}$$

$$\begin{aligned}&r_2+\sqrt{r_2^2-r_m^2}=\sqrt{2z_2^2+r_0^2}\\&+\sqrt{2}\cdot\sqrt{z_2^2-z_1^2+S^2}\end{aligned} \tag{18}$$

2.3. Symmetric trajectory formulation

Using **Equations 17 and 18**, **Equation 16** can be transformed into the following form:

$$\begin{aligned}&\sqrt{2}\{\ln(\sqrt{2z_1^2+r_0^2}+\sqrt{2}S)+\ln(\sqrt{2z_2^2+r_0^2}\\&+\sqrt{2}\sqrt{z_2^2-z_1^2+S^2})-\ln(2z_1^2+r_0^2-2S^2)\}\\&=\arcsin\frac{z_2}{\sqrt{q^2+z_1^2}}-\arcsin\frac{z_1}{\sqrt{q^2+z_1^2}}\end{aligned} \tag{19}$$

For a trajectory symmetric with respect to the r-axis, the following relations hold:

$$\begin{aligned}&z_2=-z_1=z,\ \alpha=\alpha_1,\ \frac{z}{r_c}\to z,\ \frac{S}{r_c}\to S,\\&\frac{q}{r_c}\to q,\ \mu=\frac{r_0}{r_c}\end{aligned} \tag{20}$$

where r_c is the radius of the inner cylindrical electrode. Substituting **Equation 20** into **Equation 19** gives:

$$\begin{aligned}&\sqrt{2}\left\{2\ln(\sqrt{2z^2+\mu^2}+\sqrt{2}S)\right.\\&\left.-\ln(2z^2+\mu^2-2S^2)\right\}=2\arcsin\frac{z}{\sqrt{q^2+z^2}}\end{aligned} \tag{21}$$

For the subsequent derivations, we introduce the following auxiliary functions:

$$F_1 = \ln(\sqrt{2z_1^2 + r_0^2} + \sqrt{2}S) \tag{22}$$

$$F_2 = \ln(\sqrt{2z_1^2 + r_0^2} + \sqrt{2}\sqrt{z_2^2 - z_1^2 + S^2}) \tag{23}$$

$$F_3 = \ln(2z_1^2 + r_0^2 - 2S^2) \tag{24}$$

$$f_1 = \arcsin\frac{z_1}{\sqrt{q^2 + z_1^2}} \tag{25}$$

$$f_2 = \arcsin\frac{z_2}{\sqrt{q^2 + z_1^2}} \tag{26}$$

2.4. First-order sensitivity relations

The relations derived above define the nominal charged-particle trajectory for a prescribed set of geometric and entrance parameters. For parameter optimization, however, it is also necessary to determine how the exit coordinates and trajectory angle respond to small variations in the entrance angle. The derivatives derived below therefore constitute the first-order sensitivity relations used subsequently to formulate the angular-focusing and collimation conditions. This analytical sensitivity formulation avoids repeated numerical tracing of neighboring trajectories during the parameter-search procedure.

We next determine the derivatives of the introduced functions with respect to the entrance angle α:

$$\frac{dF_1}{d\alpha} = \frac{\dfrac{2z_1\dfrac{dz_1}{d\alpha}}{\sqrt{2z_1^2 + r_0^2}} + \sqrt{2}q}{\sqrt{2z_1^2 + r_0^2} + \sqrt{2}S} \tag{27}$$

$$\frac{dF_2}{d\alpha} = \frac{\dfrac{2z_2\dfrac{dz_2}{d\alpha}}{\sqrt{2z_2^2 + r_0^2}} + \dfrac{\sqrt{2}\left(z_2\dfrac{dz_2}{d\alpha} - z_1\dfrac{dz_1}{d\alpha} + Sq\right)}{\sqrt{z_2^2 - z_1^2 + S^2}}}{\sqrt{2z_2^2 + r_0^2} + \sqrt{2}\sqrt{z_2^2 - z_1^2 + S^2}} \tag{28}$$

After algebraic simplification, **Equation 28** becomes:

$$\frac{dF_2}{d\alpha} = \frac{2z_2\dfrac{dz_2}{d\alpha}}{\sqrt{2z_2^2 + r_0^2}\cdot\sqrt{2}\sqrt{z_2^2 - z_1^2 + S^2}} + \frac{\sqrt{2}\left(Sq - z_1\dfrac{dz_1}{d\alpha}\right)}{\sqrt{z_2^2 - z_1^2 + S^2}\left(\sqrt{2z_2^2 + r_0^2} + \sqrt{2}\sqrt{z_2^2 - z_1^2 + S^2}\right)} \tag{29}$$

The derivative of F_3 with respect to α is given by:

$$\frac{dF_3}{d\alpha} = 4\frac{z_1\dfrac{dz_1}{d\alpha} - Sq}{2z_1^2 + r_0^2 - 2S^2} \tag{30}$$

For the trajectory symmetric with respect to the r-axis and defined by **Equation 20**, **Equations 27**, **29**, **and 30** reduce to:

$$\frac{dF_1}{d\alpha} = \frac{\dfrac{-2z\dfrac{dz_1}{d\alpha}}{\sqrt{2z^2 + \mu^2}} + \sqrt{2}q}{\sqrt{2z^2 + \mu^2} + \sqrt{2}S} \tag{31}$$

$$\frac{dF_2}{d\alpha} = \frac{\sqrt{2}z\dfrac{dz_2}{d\alpha}}{S\sqrt{2z^2 + \mu^2}} + \sqrt{2}\frac{Sq + z\dfrac{dz_1}{d\alpha}}{S\left(\sqrt{2z^2 + \mu^2} + \sqrt{2}S\right)} \tag{32}$$

$$\frac{dF_3}{d\alpha} = -4\frac{z\dfrac{dz_1}{d\alpha} + Sq}{2z^2 + \mu^2 - 2S^2} \tag{33}$$

The derivatives of the functions f_1 and f_2 with respect to α are then determined as follows:

$$\sin f_1 = \frac{z_1}{\sqrt{q^2 + z_1^2}} \tag{34}$$

$$\frac{df_1}{d\alpha}\cos f_1 = \frac{\left(q^2 + z_1^2\right)\dfrac{dz_1}{d\alpha} - z_1^2\dfrac{dz_1}{d\alpha} + qSz_1}{\left(q^2 + z_1^2\right)^{\frac{3}{2}}} \tag{35}$$

$$\cos f_1 = \frac{q}{\sqrt{q^2 + z_1^2}} \tag{36}$$

$$\frac{df_1}{d\alpha} = \frac{1}{\cos f_1}\frac{q^2\dfrac{dz_1}{d\alpha} + qSz_1}{\left(q^2 + z_1^2\right)^{\frac{3}{2}}} \tag{37}$$

$$\frac{df_1}{d\alpha} = \frac{q\dfrac{dz_1}{d\alpha} + Sz_1}{q^2 + z_1^2} \tag{38}$$

Using **Equation 20**, **Equation 38** becomes:

$$\frac{df_1}{d\alpha} = \frac{q\dfrac{dz_1}{d\alpha} - Sz}{q^2 + z^2} \tag{39}$$

Similarly, the derivative of $\frac{df_2}{d\alpha}$ is obtained as follows:

$$\sin f_2 = \frac{z_2}{\sqrt{q^2 + z_1^2}} \tag{40}$$

$$\cos f_2 = \frac{\sqrt{z_1^2 - z_2^2 + q^2}}{\sqrt{q^2 + z_1^2}} \tag{41}$$

$$\frac{df_2}{d\alpha} = \frac{1}{\cos f_2} \frac{\left(q^2 + z_1^2\right)\frac{dz_2}{d\alpha} - z_1 z_2 \frac{dz_1}{d\alpha} + qSz_2}{\left(q^2 + z_1^2\right)^{\frac{3}{2}}} \tag{42}$$

and, after simplification:

$$\frac{df_2}{d\alpha} = \frac{\left(q^2 + z_1^2\right)\frac{dz_2}{d\alpha} - z_1 z_2 \frac{dz_1}{d\alpha} + qSz_2}{\left(q^2 + z_1^2\right)\sqrt{z_1^2 - z_2^2 + q^2}} \tag{43}$$

For the symmetric trajectory, this expression reduces to:

$$\frac{df_2}{d\alpha} = \frac{\left(q^2 + z^2\right)\frac{dz_2}{d\alpha} + z^2 \frac{dz_1}{d\alpha} + qSz}{q\left(q^2 + z^2\right)} \tag{44}$$

Substituting the derivatives $\frac{dF_1}{d\alpha}$, $\frac{dF_2}{d\alpha}$, $\frac{dF_3}{d\alpha}$, $\frac{df_1}{d\alpha}$, and $\frac{df_2}{d\alpha}$ obtained from **Equations 27, 29, 30, 38, and 43** into the derivative with respect to α, we obtain the derivative of the exit coordinate z_2. To simplify the notation, we introduce:

$$A_1 = \sqrt{2z_1^2 + r_0^2}, \quad A_2 = \sqrt{2z_2^2 + r_0^2},$$
$$G = \sqrt{z_2^2 - z_1^2 + S^2}, \quad N = \sqrt{q^2 + z_1^2 - z_2^2}, \tag{45}$$
$$D = 2z_1^2 + r_0^2 - 2S^2, \quad \frac{dz_2}{d\alpha} = \frac{L\frac{dz_1}{d\alpha} + M}{K}$$

where:

$$K = \frac{1}{N} - \frac{2z_2}{A_2 G},$$

$$L = \frac{2\sqrt{2}z_1}{A_1\left(A_1 + \sqrt{2}S\right)} - \frac{2z_1}{G\left(A_2 + \sqrt{2}G\right)} - \frac{4\sqrt{2}z_1}{D} + \frac{z_1 z_2}{\left(q^2 + z_1^2\right)N} + \frac{q}{q^2 + z_1^2} \text{ and}$$

$$M = \frac{2q}{A_1 + \sqrt{2}S} + \frac{2Sq}{G\left(A_2 + \sqrt{2}G\right)} + \frac{4\sqrt{2}Sq}{D} - \frac{qSz_2}{\left(q^2 + z_1^2\right)N} + \frac{Sz_1}{q^2 + z_1^2}$$

We now determine $\frac{dz_2}{d\alpha}$ for the trajectory symmetric with respect to the *r*-axis and defined by **Equation 20**. Using the corresponding derivatives from **Equations 31–33, 39, and 44**, and performing the necessary algebraic transformations, we obtain:

$$\frac{dz_2}{d\alpha} = \frac{qSR}{SR - 2zq}\left(L\frac{dz_1}{d\alpha} + M\right) \tag{46}$$

where $R = \sqrt{2z^2 + \mu^2}$, and L and M are given by **Equation 45** evaluated using **Equation 20**.

Next, we derive the derivative $\frac{d\alpha_1}{d\alpha}$, which is required for the subsequent focusing analysis. From the equation of the equipotential surface (**Equation 3**), we have:

$$r_2^2 - r_1^2 = 2z_2^2 - 2z_1^2 \tag{47}$$

$$S^2 + \frac{r^2}{2} - \frac{r_1^2}{2} = S^2 + z^2 - z_1^2 \tag{48}$$

For point B in **Figure 1**, the following geometrical relation can be written:

$$\cot\alpha_1 = \left.\frac{dz}{dr}\right|_{Z=Z_2} = \sqrt{\frac{q^2 + z_1^2 - z_2^2}{S^2 + z_2^2 - z_1^2}} \tag{49}$$

Differentiating **Equation 49** with respect to α and taking into account that $\frac{dS}{d\alpha} = q$ and $\frac{dq}{d\alpha} = -S$, we obtain:

$$-\left(1 + \cot^2\alpha_1\right)\frac{d\alpha_1}{d\alpha} = \frac{1}{S^2 + z_2^2 - z_1^2}$$
$$\times\left[\frac{z_1\frac{dz_1}{d\alpha} - qS - z_2\frac{dz_2}{d\alpha}}{\sqrt{q^2 + z_1^2 - z_2^2}}\sqrt{S^2 + z_2^2 - z_1^2}\right. \tag{50}$$
$$\left. - \frac{Sq + z_2\frac{dz_2}{d\alpha} - z_1\frac{dz_1}{d\alpha}}{\sqrt{S^2 + z_2^2 - z_1^2}}\sqrt{q^2 + z_1^2 - z_2^2}\right]$$

$$\frac{d\alpha_1}{d\alpha} = -\frac{1}{1+\cot^2\alpha_1}\cdot\frac{1}{(S^2+z_2^2-z_1^2)^{\frac{3}{2}}(q^2+z_1^2-z_2^2)^{\frac{1}{2}}}$$
$$\times\left\{\left(z_1\frac{dz_1}{d\alpha}-qS-z_2\frac{dz_2}{d\alpha}\right)\left(S^2+z_2^2-z_1^2\right)\right. \quad (51)$$
$$\left.-\left(qS+z_2\frac{dz_2}{d\alpha}-z_1\frac{dz_1}{d\alpha}\right)\cdot\left(q^2+z_1^2-z_2^2\right)\right\}$$

Expanding the terms and collecting like terms yields:

$$\frac{d\alpha_1}{d\alpha} = -\frac{1}{1+\cot^2\alpha_1}\cdot\frac{\left(S^2+q^2\right)\left(z_1\frac{dz_1}{d\alpha}-z_2\frac{dz_2}{d\alpha}-qS\right)}{\left(S^2+z_2^2-z_1^2\right)^{\frac{3}{2}}\left(q^2+z_1^2-z_2^2\right)^{\frac{1}{2}}} \quad (52)$$

Since $1+\cot^2\alpha_1 = \frac{S^2+q^2}{S^2+z_2^2-z_1^2}$, **Equation 52** can be rewritten as:

$$\frac{d\alpha_1}{d\alpha} = \frac{qS+z_2\frac{dz_2}{d\alpha}-z_1\frac{dz_1}{d\alpha}}{\left(S^2+z_2^2-z_1^2\right)^{\frac{1}{2}}\left(q^2+z_1^2-z_2^2\right)^{\frac{1}{2}}} \quad (53)$$

For the symmetric trajectory defined by **Equation 20**, **Equation 53** reduces to:

$$\frac{d\alpha_1}{d\alpha} = 1+\frac{z}{Sq}\left(\frac{dz_2}{d\alpha}+\frac{dz_1}{d\alpha}\right) \quad (54)$$

3. Feasible-domain identification and parameter-space reduction

3.1. Selection of the hyperbolic electrode parameter

The geometrical pre-screening stage acts as a feasibility filter and eliminates parameter combinations for which particles either fail to enter the deflecting field or cannot subsequently cross the hyperbolic electrode at the exit.

Figure 2 illustrates different configurations of the hyperbolic electrode for various values of the parameter μ. Considering a suitable penetration depth of charged particles into the electrostatic field and reduced influence of the hyperbolic electrode mesh cells, $\mu = 0.8$ was selected as a representative configuration for the geometric pre-screening analysis described in Section 3.2. This choice does not preclude other admissible values of μ; in Section 4, the successive-approximation algorithm is additionally applied to $\mu = 0.6$ and $\mu = 0.7$ to assess the sensitivity of the focusing and collimation conditions to the curvature of the hyperbolic electrode, with $\mu = 0.8$ retained as the practically preferred configuration.

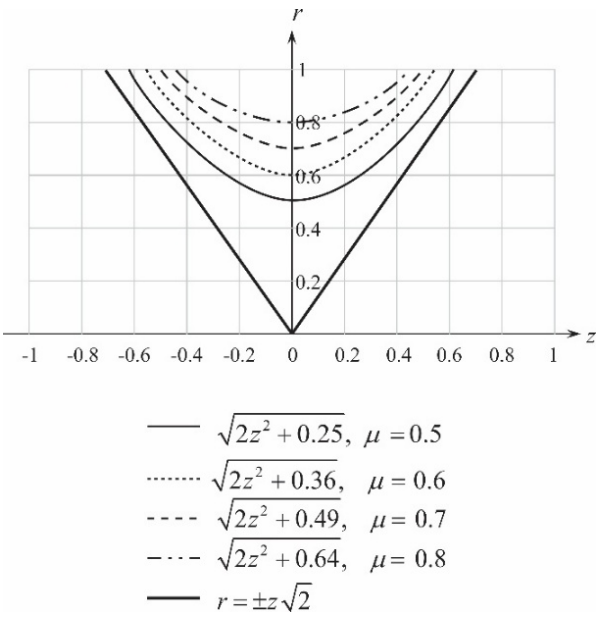


Figure 2. Hyperbolic electrode configurations for different values of the parameter μ. From bottom to top, the curves correspond to $\mu = 0.5$, 0.6, 0.7, and 0.8; the straight lines $r = \pm\sqrt{2}z$ show the conical electrodes.

3.2. Preliminary analysis of particle trajectories

Numerical evaluation of the derived analytical expressions is difficult because several algebraic functions have restricted domains. To improve computational efficiency and determine suitable conditions for the transmission of charged-particle trajectories, different penetration geometries of the particle beam into the deflecting field region of the HM were considered. The HM is intended to serve as an intermediate element between two stages of a cylindrical mirror system.

It should be noted that the region between the inner cylindrical electrode, maintained at zero potential, and the hyperbolic electrode is field-free. Consequently, the particle trajectories within this region are straight-line segments. The equation of a straight line can be written as $r = kz + b$, where the coefficient k is determined by the inclination angle of the trajectory. This property enables a preliminary geometrical analysis to be performed, thereby reducing the parameter domain required for subsequent numerical calculations.

Figure 3 shows the penetration of charged-particle trajectories through the hyperbolic electrode for entrance angles from 40° to 60°.

As shown in the figure, at b = 0.5 and entrance angles of 40° and 45°, the trajectories do not enter the deflecting-field region of the HM, whereas at 50°, the trajectory passes in proximity to the hyperbolic electrode over a relatively long section, which is undesirable.

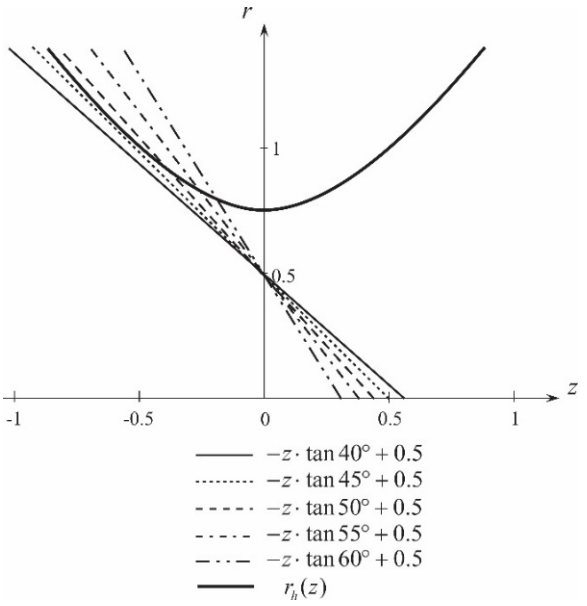


Figure 3. Charged-particle trajectories entering the hyperbolic electrostatic mirror at b = 0.5 for different entrance angles. The slope of the trajectories increases with the entrance angle from α = 40° (solid line) to α = 60° (dash-dotted line).

Figure 4 shows the trajectories at a fixed entrance angle of 40° for different values of b. The trajectories with b = 0.5 and b = 0.6 do not intersect the hyperbolic electrode, whereas the trajectory with b = 0.7 enters the field region at z ≈ −0.15. For b = 0.8, the trajectory passes through the vertex of the hyperbolic electrode, and for b = 0.9, it enters the field in the right half of the HM ($z > 0$). In these two cases, a symmetric exit through the hyperbolic electrode is impossible; therefore, they were excluded from further consideration.

Figure 5 shows trajectory configurations for different values of b and α. As shown in the figure, the most favorable configurations for μ = 0.8 lie within the entrance-angle range of 45°–50° for b = 0.6–0.7.

Thus, consideration of the charged-particle trajectories in the region between the inner cylindrical electrode and the hyperbolic electrode, i.e., outside the field region, where the trajectory segments are straight lines, made it possible to significantly reduce the computational domain for determining the electron-optical characteristics of the combined system consisting of cylindrical, hyperbolic, and cylindrical mirrors.

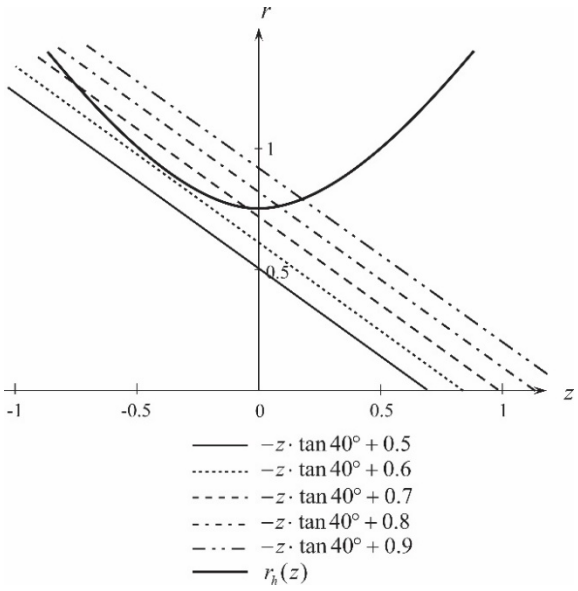


Figure 4. Charged-particle trajectories entering the hyperbolic electrostatic mirror at a fixed entrance angle α = 40° for different values of b. From bottom to top, the trajectories correspond to b = 0.5, 0.6, 0.7, 0.8, and 0.9.

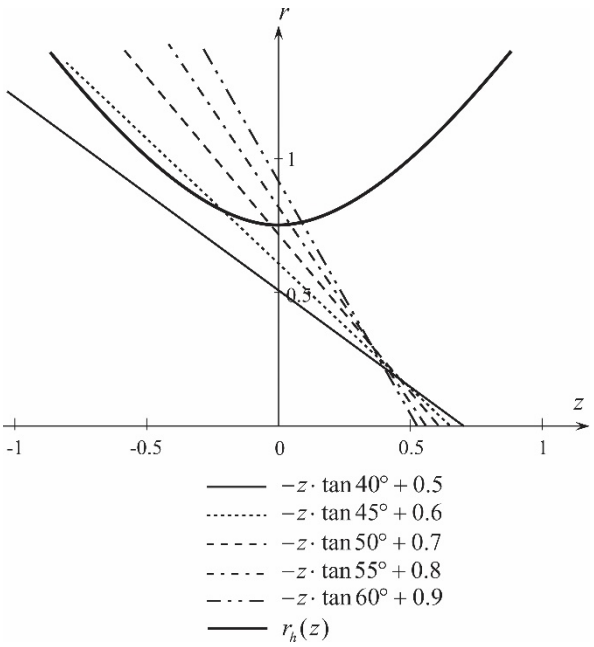


Figure 5. Charged-particle trajectories entering the hyperbolic electrostatic mirror for different values of b and entrance angles α. The slope of the trajectories increases from (α = 40°, b = 0.5) to (α = 60°, b = 0.9).

To quantify the geometric pre-screening of trajectories and confirm the reduced computational domain, the entrance coordinates z_α, along with the corresponding profile radii $r_h(z_\alpha)$ and $r(z_\alpha,\alpha)$ were evaluated for $\mu = 0.8$ across various values of parameter $b \in [0.6, 0.9]$ and entrance angles $\alpha \in [45°, 60°]$. The key numerical results obtained via iterative root-finding are summarized in **Table 1**.

Here, the function:

$$\Phi(z_\alpha,\alpha) = r_h(z_\alpha) - r(z_\alpha,\alpha) \tag{55}$$

represents the difference between the hyperbolic-electrode profile $r_h(z_\alpha)$ and the particle-trajectory radius $r(z_\alpha,\alpha)$ at a given axial coordinate *z*. A parameter combination is regarded as geometrically admissible only if the corresponding trajectory intersects the hyperbolic electrode in the required half-space and subsequently permits a symmetric exit from the mirror. The geometrical analysis therefore acts as a feasibility constraint applied before the electron-optical focusing or collimation conditions are solved.

The intersection coordinate z_α was obtained as the root of $\Phi(z_\alpha,\alpha) = 0$, identified using the successive-approximation method. The absolute residuals reported in **Table 1** remained below 10^{-3}, confirming convergence of the iterative root-finding procedure used to determine the intersection coordinate z_α.

As shown in **Table 1**, for $b = 0.8$, the beam entered exactly at the vertex of the hyperbolic surface ($z_\alpha = 0, r = 0.8$), whereas for $b = 0.9$, the intersection points shifted into the positive half-space ($z_\alpha > 0$). This confirms that configurations with $b \geq 0.8$ prevent symmetric beam exit and are therefore excluded from the admissible domain considered for the symmetric operating configuration.

4. Successive-approximation method for parameter determination

The analytical relations derived in Section 2, together with the parameter ranges established in Section 3, involve transcendental equations that cannot be solved in closed form for the parameters of practical interest. The method of successive

Table 1. Trajectory intersection parameters at the hyperbolic electrode for μ = 0.8

b	α	z_α	$r_h(z_a)$	$r_h(z_\alpha)$	$\Phi(z_\alpha,\alpha)$
0.6	45	−0.316	0.916	0.916	4.966×10^{-4}
	50	−0.214	0.855	0.855	5.341×10^{-4}
	55	−0.163	0.832	0.832	8.815×10^{-5}
	60	−0.127	0.820	0.820	1.504×10^{-5}
0.7	45	−0.117	0.817	0.817	5.427×10^{-5}
	50	−0.092	0.810	0.810	9.266×10^{-4}
	55	−0.075	0.806	0.807	4.298×10^{-4}
	60	−0.060	0.804	0.805	1.931×10^{-4}
0.8	45–60	0	0.800	0.800	0
0.9	45	0.090	0.810	0.810	-1.135×10^{-5}
	50	0.077	0.807	0.808	-6.239×10^{-4}
	55	0.066	0.805	0.806	-3.184×10^{-4}
	60	0.055	0.804	0.804	-1.525×10^{-4}

Note: All lengths are normalized with r_c; α is given in degrees.

approximations was therefore used to construct computational algorithms for determining the electron-optical parameters of the system in two operating regimes: first-order angular focusing and first-order beam collimation.

4.1. Algorithm for the focusing regime

The algorithm for the focusing regime is:

1. Set the electrode parameter μ, the entrance angle α, the trajectory parameter S, and the entrance coordinate z_1.
2. Compute $q = S \cdot \cot\alpha$ (**Equation 8**).
3. Determine the exit coordinate z_2 from **Equation 19** by successive approximations.
4. Compute the derivatives $\frac{dz_2}{d\alpha}$ (**Equation 45**) and $\frac{d\alpha_1}{d\alpha}$ (**Equation 53**).
5. Using these derivatives, determine the parameter P from the first-order angular-focusing condition of the complete cylindrical–hyperbolic–cylindrical system by successive approximations, where P is the reflection parameter of the cylindrical mirror stage.[1]

4.2. Algorithm for the collimation regime

The algorithm for the collimation regime is analogous to that described in Section 4.1 (Steps 1–4), but in Step 5 the parameter P was determined from the first-order collimation condition, which requires the exit angle to be independent of the entrance angle, $\frac{d\alpha_1}{d\alpha} = 0$. For the symmetric trajectory, according to **Equation 54**, this condition yields:

$$1 + \frac{z}{Sq}\left(\frac{dz_2}{d\alpha} + \frac{dz_1}{d\alpha}\right) = 0 \tag{56}$$

The angular energy dispersion of the system was then evaluated for the converged parameter set. Both algorithms were implemented computationally, and the resulting electron-optical parameters were obtained for the range of μ, S (or b), and α values discussed in Section 3. The search was initialized only within the feasible domain identified in Section 3; therefore, parameter combinations corresponding to non-transmitting trajectories were not evaluated during the iterative stage.

4.3. Numerical results and discussion

Although Section 3 identified $\mu = 0.8$ as the practically preferred electrode configuration, the successive-approximation algorithm imposes no inherent restriction on μ. To evaluate the sensitivity of the focusing and collimation solutions to electrode curvature, additional computations were performed for $\mu = 0.6$ and $\mu = 0.7$ within the reduced parameter domain established in Section 3.

The proposed successive-approximation algorithms were applied to determine the electron-optical trajectory parameters for various mirror configurations. Computations were carried out across electrode geometry parameters $\mu \in \{0.6, 0.7, 0.8\}$, entrance angles $\alpha \in [30°, 45°]$, and trajectory parameters $S \in [0.3, 0.4]$. For each pair (μ, α), the entrance coordinates z_1 were taken within the geometrically admissible range determined using the same pre-screening procedure as in Section 3.2.

The exit coordinates z_2 computed for prescribed entrance coordinates z_1 are given in Table S1, and a representative selection is summarized in **Table 2**.

Table 2. Exit coordinate z_2 of the trajectory in the hyperbolic electrostatic mirror obtained from Equation 19 through successive approximations for S = 0.3 and prescribed values of μ, α, and the entrance coordinate z_1 (lengths normalized by r_c; α in degrees)

μ	α	z_1	z_2
0.6	45	−0.27	0.4034
		−0.30	0.4160
0.7	40	−0.24	0.4303
		−0.28	0.4437
		−0.30	0.4434
0.7	45	−0.21	0.3645
		−0.24	0.3735
		−0.27	0.3716
		−0.30	0.3429
0.8	40	−0.20	0.4036
		−0.24	0.4060
		−0.27	0.3943
		−0.30	0.3497
	45	−0.15	0.3314
		−0.19	0.3365
		−0.24	0.3203
		−0.26	0.2970

Table 2 shows that, for fixed μ and α, the exit coordinate z_2 depends non-monotonically on the entrance coordinate z_1: for μ = 0.8 and α = 45°, z_1 increased from 0.3314 at $z_1 = -0.15$ to 0.3365 at $z_1 = -0.19$ and then decreased to 0.2970 at $z_1 = -0.26$. At a fixed entrance point, z_2 decreased with increasing entrance angle (for μ = 0.8 and $z_1 = -0.24$, from 0.4060 at α = 40° to 0.3203 at α = 45°) and with increasing electrode parameter μ (at α = 45°, from 0.4034 for μ = 0.6 to 0.3716 for μ = 0.7 at $z_1 = -0.27$, and from 0.3735 for μ = 0.7 to 0.3203 for μ = 0.8 at $z_1 = -0.24$).

The results demonstrate that the geometrical pre-screening and iterative stages perform complementary functions. The first stage eliminates parameter combinations that cannot produce physically admissible symmetric trajectories, whereas the second stage determines the operating point satisfying the prescribed electron-optical condition. Consequently, the iterative search is performed over a substantially smaller domain than would be required in direct parameter scanning.

4.4. Advantages and limitations in practical applications

The proposed method offers several practical advantages for the design of energy analyzers with a hyperbolic mirror. First, because the particle trajectories in the HM were described in closed form and the first-order sensitivities are obtained analytically, the electron-optical properties can be evaluated without numerical field calculations or tracing neighboring trajectories. Second, the geometric pre-screening is based only on straight-line trajectory segments and the equation of the hyperbolic electrode; it is therefore computationally inexpensive and excludes non-transmitting configurations before any iterative calculation is performed (**Table 1**). Third, the iterative stage is low-dimensional: for prescribed μ, α, S, and z_1, only the exit coordinate z_2 is found from the single transcendental **Equation 19**, and only the parameter P of the cylindrical mirror stage is then determined from the focusing or collimation condition. Fourth, the explicit dependence of the results on the electrode parameter, the entrance angle, and the entrance coordinate makes the influence of each design parameter transparent (**Table 2**), which is useful when choosing the electrode curvature and the beam entrance conditions at the preliminary design stage. Finally, Steps 1–4 of the algorithm are common to the focusing and collimation regimes, so both regimes can be analyzed within the same framework.

It is useful to compare the present approach with the classical methods of charged-particle optics. In the textbooks by Liebl[26] and Wollnik,[27] the properties of electrostatic and magnetic elements are described by expanding the trajectories in power series about a reference trajectory; the expansion coefficients form transfer matrices, and the first-order coefficients determine the focusing and dispersion of the system. The present method differs in that the particle trajectories in the hyperbolic field are obtained in closed form, without a paraxial expansion, and the first-order coefficients are then identified using direct differentiation of the exact solution with respect to the entrance angle. In this sense, the derivatives $\frac{dz_2}{d\alpha}$ and $\frac{d\alpha_1}{d\alpha}$ (**Equations 45, 46, 53, and 54**) are the first-order position–angle and angle–angle elements of the transfer matrix of the HM. The method can therefore be adapted to the matrix formalism. If the derivatives with respect to the particle energy are calculated in the same way, they give the dispersion elements, and the resulting matrix of the HM can be multiplied by the known matrices of the cylindrical mirror stages. This is the approach used by Yavor *et al.*[28] in the ion-optical design of multiple-reflection time-of-flight systems. Such a combination would allow the complete cylindrical–hyperbolic–cylindrical system to be analyzed by matrix multiplication rather than by solving the combined equations, which would further increase the computational efficiency.

The method also has limitations that should be considered in practical applications. The analysis assumes an ideal field formed using hyperbolic and conical electrodes of unlimited extent; fringing fields at the electrode edges, the finite size of the electrodes, and manufacturing tolerances are not included. The hyperbolic electrode through which the beam passes must be made as a mesh, and the field perturbation and transmission losses introduced by the mesh cells are not described by the model. The treatment is restricted to non-relativistic particle motion along symmetric meridional trajectories and to first-order properties; second-order aberrations, skew trajectories, and space-charge effects are not considered, so the energy resolution and luminosity of the complete analyzer cannot yet be estimated quantitatively. In addition, the successive-approximation procedure requires initial values within the admissible domain, and

the results have not yet been verified by direct numerical trajectory simulation or experiment. The method is therefore best suited for the preliminary synthesis of analyzer schemes, whose parameters should subsequently be refined by full numerical modeling.

5. Conclusion

This study addressed whether the electron-optical parameters of an HM, in which the beam enters and exits through the hyperbolically shaped electrode, can be determined without broad numerical trajectory scanning. The results show that this is possible: by combining a closed-form trajectory solution with a geometric feasibility filter and a successive-approximation procedure, the search for first-order angular-focusing and collimation regimes was reduced to a low-dimensional iterative problem over a small, physically admissible parameter domain.

The main findings are as follows. First, because the potential of the HM is quadratic in r and z, the equations of motion separate and admit an exact solution. This yields closed-form relations linking the entrance and exit coordinates of a trajectory to the electrode parameter μ, the entrance angle α, and the trajectory parameter S (**Equations 19–21**). Second, differentiation of these relations with respect to α gives the first-order sensitivity relations for the exit coordinate and the exit angle in explicit form (**Equations 45, 46, 53, and 54**). For the symmetric trajectory, the exit-angle sensitivity reduces to the compact expression (**Equation 54**), from which the collimation condition (**Equation 56**) follows directly. These relations replace the numerical tracing of neighboring trajectories that would otherwise be required to evaluate the focusing properties.

Third, the geometric pre-screening of the straight-line trajectory segments in the field-free region established clear admissibility limits for the beam entrance conditions. For $\mu = 0.8$, trajectories with $b = 0.5$ do not reach the deflecting field at $\alpha = 40°$–$45°$. For $b = 0.8$, the beam enters exactly at the vertex of the hyperbolic electrode, and for b = 0.9, the entrance point shifts into the positive half-space ($z_\alpha = 0.055$-0.090 for $\alpha = 45°$–$60°$); in both cases, a symmetric exit is impossible. Admissible entrance points were obtained for b = 0.6–0.7, i.e., for b < μ, with z_α ranging from –0.316 to –0.060 (**Table 1**), and the intersection coordinates were determined with residuals below 10^{-3}. Consequently, parameter combinations corresponding to non-transmitting trajectories were excluded before any electron-optical condition was evaluated.

Fourth, the successive-approximation calculations of the exit coordinate (**Table 2**) revealed systematic trends. For a fixed entrance point, the exit coordinate z_2 decreases with increasing entrance angle α and electrode parameter μ; for example, for $\mu = 0.8$ and $z_1 = -0.24$, z_2 decreases from 0.4060 at $\alpha = 40°$ to 0.3203 at $\alpha = 45°$. For fixed μ and α, z_2 depends non-monotonically on z_1 and passes through a maximum. These dependences provide practical guidelines for selecting the electrode curvature and the beam entrance conditions.

The significance of this work lies in the following. To the best of our knowledge, it provides the first analytical treatment of first-order focusing and collimation in an HM with the beam passing through the hyperbolic electrode, a configuration for which only numerical studies have previously been reported. The proposed two-stage scheme, consisting of analytical feasibility screening followed by low-dimensional iteration, preserves the physical transparency of the analytical model, avoids three-dimensional field calculations, and supplies well-defined initial approximations for the synthesis of compact, high-luminosity cylindrical–hyperbolic–cylindrical energy analyzers for space and plasma diagnostics. The same approach can be extended to other electrostatic systems whose fields admit closed-form trajectory solutions.

The limitations of the present analysis are summarized in Section 4.4; future work will address the representation of the HM in transfer-matrix form,[26-28] second-order focusing, the energy resolution and luminosity of the complete cylindrical–hyperbolic–cylindrical system, and verification of the analytical results using direct numerical trajectory simulation.

Acknowledgments

None.

Funding

This research was funded by the Science Committee of the Ministry of Science and Higher Education of the Republic of Kazakhstan (Grant No. AP26101393).

Conflict of interest

The authors declare no conflicts of interest.

Author contributions:

Conceptualization: Arman Saulebekov
Investigation: Arman Saulebekov, Zhanar Kambarova, Meiramkul Tungushbekova, Tilektes Shugayeva
Methodology: Arman Saulebekov, Zhanar Kambarova
Writing–original draft: Arman Saulebekov, Zhanar Kambarova, Meiramkul Tungushbekova, Tilektes Shugayeva
Writing–review & editing: Arman Saulebekov, Zhanar Kambarova, Meiramkul Tungushbekova, Tilektes Shugayeva

Availability of data

The datasets and code generated or analyzed during the current study are available from the corresponding author upon reasonable request.

AI tools statement

The authors confirmed that no AI tools were used in the preparation of this work.

References

1. Ashimbaeva BU, Chokin KSh, Saulebekov AO, Kambarova ZhT. The combined energy analyzer composed of electrostatic mirror fields. *J Electron Spectros Relat Phenomena*. 2012;185(11):518-522.

   https://doi.org/10.1016/j.elspec.2012.10.008

2. Kambarova ZhT, Saulebekov AO, Kopbalina KB. Calculation of the electron-optical scheme of a new type mirror energy analyzer of charged particles. *Bull Karaganda Univ Phys*. 2022;106(2):49-57.

   https://doi.org/10.31489/2022PH2/49-57

3. Kambarova ZhT, Saulebekov AO, Kassymov SS. A novel design of an energy analyzer for charged particles based on a non-uniform electrostatic field. *Eurasian Phys Tech J*. 2025;22(3):148-155.

   https://doi.org/10.31489/2025N3/148-155

4. Spivak-Lavrov IF, Shugayeva TZh, Seiten AB, Amantaeva ASh. Analytical description of the electrostatic field of multiple system based on a conducting circular cylinder. *J Electrostat*. 2026;140:104249.

   https://doi.org/10.1016/j.elstat.2026.104249

5. Yang S, Xu L, Yin J, Wang H, Li B. Fast finite element electrostatic analysis with domain decomposition method. *IEICE Electron Express*. 2023;20(5):20220540.

   https://doi.org/10.1587/elex.20.20220540

6. Read FH, Bowring NJ. The CPO programs and the BEM for charged particle optics. *Nucl Instrum Methods Phys Res A*. 2011;645:273-277.

   https://doi.org/10.1016/j.nima.2010.12.163

7. Vallette A, Indelicato P. Analytical study of electrostatic ion beam traps. *Phys Rev Spec Top Accel Beams*. 2010;13(11):114001.

   https://doi.org/10.1103/PhysRevSTAB.13.114001

8. Gonzalez-Lizardo A, Ulloa-Dávila E, Leal-Quiros E. Simulation of a hyperbolic field energy analyzer. In: *Proceedings of the 16th Latin American Workshop on Plasma Physics (LAWPP)*. Piscataway, NJ: IEEE; 2017:52-55.

   https://doi.org/10.1109/LAWPP.2017.8692187

9. Leal-Quiros E, Prelas MA. A hyperbolic energy analyzer. *Rev Sci Instrum*. 1990;61(6):1708-1712.

   https://doi.org/10.1063/1.1141136

10. Hesam Mahmoudi Nezhad N, Ghaffarian Niasar M, Hagen CW, Kruit P. A new approach for fast field calculation in electrostatic electron lens design and optimization. *Sci Rep*. 2024;14:4859.

    https://doi.org/10.1038/s41598-024-55518-3

11. Yao K, Ma W, Huang H, Li G, Ding Z, Liu J. A fast and accurate method for multi-electrode electrostatic lens design. *IEEE J Electron Devices Soc*. 2026;14:311-317.

    https://doi.org/10.1109/JEDS.2026.3693909

12. Gorelik V. Optimization of cylindrical mirror analyzer. *J Electron Spectros Relat Phenomena*. 2023;264:147315.

    https://doi.org/10.1016/j.elspec.2023.147315

13. Hoffstaetter GH. Successive approximations for charged particle motion. *Ultramicroscopy*. 2000;81(3-4):111-121.

    https://doi.org/10.1016/S0304-3991(99)00186-2

14. Sabouri A, Perez-Martinez CS. Design of electrostatic lenses through genetic algorithm and particle swarm optimisation methods integrated with differential algebra. *Ultramicroscopy*. 2024;266:114024.

    https://doi.org/10.1016/j.ultramic.2024.114024

15. Sise O, Ulu M, Dogan M, Martinez G, Zouros TJM. Fringing field optimization of hemispherical deflector analyzers using BEM and FDM. *J Electron Spectros Relat Phenomena*. 2010;177(1):42-51.

    https://doi.org/10.1016/j.elspec.2010.01.003

16. Isik N, Ince M. Determination of electron trajectories within an energy analyzer using by a genetic algorithm method. *Optik*. 2022;260:169076.

https://doi.org/10.1016/j.ijleo.2022.169076

17. Kambarova Zh, Saulebekov A, Trubitsyn A. Numerical search for time-of-flight focusing conditions and its application to the analysis of TOF mass analyzer schemes. *Eng Res Express*. 2024;6(1):015037.

https://doi.org/10.1088/2631-8695/ad1c0a

18. Brais CJ, Ray SJ. A convolution approach to calculating the m/z-dependent mass analyzer response in orthogonal acceleration time-of-flight mass spectrometers. *Int J Mass Spectrom*. 2022;471:116734.

https://doi.org/10.1016/j.ijms.2021.116734

19. Sachenko VD, Antonov AS, Gall LN, Berdnikov AS. Optimization of vertical acceptance of the static mass analyzer. *J Anal Chem*. 2020;75(13):1660-1664.

https://doi.org/10.1134/S1061934820130122

20. Odintsov DD, Poteshin SS. Comparison of the results of the aberration approach for the calculation of electrostatic TOF mass analyzers with simulation in SIMION. *Int J Mass Spectrom*. 2026;519:117526.

https://doi.org/10.1016/j.ijms.2025.117526

21. Turtia SB, Satchenko VD, Berdnikov AS, Compagner A. Multi-criteria approach in optimization of the optical schemes for magnet mass analyzers. *Nucl Instrum Methods Phys Res A*. 1999;427(1-2):382-386.

https://doi.org/10.1016/S0168-9002(98)01515-0

22. Kotana AN, Mohanty AK. Computation of Mathieu stability plot for an arbitrary toroidal ion trap mass analyser. *Int J Mass Spectrom*. 2017;414:13-22.

https://doi.org/10.1016/j.ijms.2016.11.021

23. Xie XD, Xu FX, Yang HY, Xiao Y, Jiang J, Ding CF. Structure and property of ladder electrode linear ion trap mass analyzer. *Chin J Anal Chem*. 2016;44(6):994-1000.

https://doi.org/10.1016/S1872-2040(16)60940-4

24. Rawat SS, Komal, Naudiyal A, Khajuria R. Archimedean t-norm based q-rung orthopair fuzzy Hamy mean operator with ordinal priority weights. *Intell Syst Res Appl J*. 2026;2:54-75.

https://doi.org/10.59543/f7febg22

25. Musbah J, Badi I. LLM-assisted virtual expert weight elicitation in pharmaceutical supply chains: a Z-number multi-agent framework. *Intell Syst Res Appl J*. 2026;2:27-39.

https://doi.org/10.59543/mmhqdg22

26. Liebl H. *Applied Charged Particle Optics*. Berlin, Germany: Springer; 2008.

https://doi.org/10.1007/978-3-540-71925-0

27. Wollnik H. *Optics of Charged Particles*. 2nd ed. London, England: Academic Press; 2021.

https://doi.org/10.1016/C2018-0-03671-3

28. Yavor MI, Plaß WR, Dickel T, Geissel H, Scheidenberger C. Ion-optical design of a high-performance multiple-reflection time-of-flight mass spectrometer and isobar separator. *Int J Mass Spectrom*. 2015;381-382:1-9.

https://doi.org/10.1016/j.ijms.2015.01.002

Arman Saulebekov *received his Doctor of Physical and Mathematical Sciences degree in 2007. He is a Professor at the Kazakhstan Branch of Lomonosov Moscow State University, Astana, Kazakhstan. His research interests include charged-particle optics.*
https://orcid.org/0000-0002-6842-9263

Zhanar Kambarova, PhD*, is a Professor at the Department of Physics and Nanotechnology, Buketov Karaganda National Research University, Kazakhstan. Her research interests include charged-particle optics, numerical modeling, and optimization of charged-particle optical systems for space and plasma applications.*
https://orcid.org/0000-0001-9808-5484

Meiramkul Tungushbekova *is a PhD student and Senior Lecturer at the Department of Physics and Nanotechnology, Buketov Karaganda National Research University, Kazakhstan. Her research interests include the development of methods and instruments for energy and mass analysis of charged particles.*
https://orcid.org/0009-0002-3410-2454

Tilektes Shugayeva, PhD*, is an Associate Professor at Heriot-Watt University Aktobe Campus, K. Zhubanov Aktobe Regional University, Kazakhstan. Her research interests include the development and optimization of time-of-flight mass analyzers.*
https://orcid.org/0000-0002-4797-4529

An International Journal of Optimization and Control: Theories & Applications (https://accscience.com/journal/ijocta)



This work is licensed under a Creative Commons Attribution 4.0 International License. The authors retain ownership of the copyright for their article, but they allow anyone to download, reuse, reprint, modify, distribute, and/or copy articles in IJOCTA, so long as the original authors and source are credited. To see the complete license contents, please visit http://creativecommons.org/licenses/by/4.0/.